Since January 2020 Elsevier has created a COVID-19 resource centre with free information in English and Mandarin on the novel coronavirus COVID-19. The COVID-19 resource centre is hosted on Elsevier Connect, the company's public news and information website.

Journal of Molecular Structure 1273 (2023) 134314

Contents lists available at ScienceDirect

Journal of Molecular Structure

journal homepage: www.elsevier.com/locate/molstr

One-pot synthesis, NMR, quantum chemical approach, molecular docking studies, drug-likeness and *in-silico* ADMET prediction of novel 1-(2,3-dihydrobenzo[b][1,4]dioxin-6-yl)-2-(furan-2-yl)-4,5-diphenyl-1*H*-imidazole derivatives

D. Rajaraman [a,*], L. Athishu Anthony [a], P. Nethaji [b], Ravali Vallangi [c]

[a] Department of Chemistry, St Joseph University, Virgin Town, Dimapur, Nagaland 797 115, India
[b] Department of Chemical Engineering, Sri Sivasubramaniya Nadar College of Engineering, Tamil Nadu 603 110, India
[c] ICAR-Central Inland Fisheries Research Institute, Barrackpore, Monirampore, Kolkata, West Bengal 700120, India

ARTICLE INFO

Article history:
Received 18 July 2022
Revised 7 October 2022
Accepted 10 October 2022
Available online 15 October 2022

Keywords:
Imidazole
DFT
Molecular docking
ADMET
Drug likeness

ABSTRACT

A novel drug to treat SARS-CoV-2 infections and hydroxyl chloroquine analogue, 1-(2,3-dihydrobenzo[b][1,4]dioxin-6-yl)-2-(furan-2-yl)-4,5-diphenyl-1*H*-imidazole (DDFDI) compound has been synthesized in one pot reaction. The novel compound DDFDI had been characterized by FT-IR, ^{1}H-NMR and ^{13}C-NMR spectral techniques. The geometrical structure was optimized by density functional theory (DFT) method at B3LYP/6-31G (d, p) as the basis set. The smaller energy value provides the higher reactivity of DDFDI compound than hydroxyl chloroquine and was corrected by high electrophilic and low nucleophilic reactions. The stability and charge delocalization of the molecule were also considered by natural bond orbital (NBO) analysis. The HOMO-LUMO energies describe the charge transfer which takes place within the molecule. Molecular electrostatic potential has also been analysed. Drug likeness and oral activity have been carried out based on Lipinski's rule of five. Molecular docking studies are implemented to analyse the binding energy of the DDFDI compound against Covid-19/6W41, COVID-19/6WCF, COVID-19/6Y84 and COVID-19/6W4B receptors and found to be considered as a better antiviral agents.

1. Introduction

In modern chemical synthesis of organic chemistry, multicomponent reactions have emerged as a powerful weapon to give a single synthetic product from the complex organic molecules. These multicomponent reactions have emerged mostly in organic synthesis and medicinal chemistry [1–3]. Multicomponent reactions are also known as tetrasubstituted compound due to their short reaction time, better efficiency, atom economy and operational simplicity [4,5].

In the current arena, interest for the synthesis of complex molecules in heterocyclic compounds, polymers, natural products, pharmaceutical and drug discovery are the new valuable approaches in MCR's [6–7]. Development of a one pot MCR's especially polysubstituted compounds have been one of the current interest method of study amongst the researchers [8].

Amongst the entire heterocyclic compound, imidazole possessed the central core due to their numerous applications as nitro groups are present in the structure [9]. Imidazole shows a wide spectrum of biological activities like antibacterial [10], antagonist [11], anti-cancer [12], anti-viral and anti-inflammatory [13], anti-oxidant [14], antifungal [15], cytotoxicity [16]. This imidazole shows great applications in natural compounds such as histamine [17], algeacidal [18], pilocarpine alkaloids [19]. In the imidazole skeleton which contain drugs are losartan (antihypertension), etomidate (hypnotic agent) and flumazenil [20]. These drugs are broadly supplied and employed. With these abundant applications of imidazole, researchers are putting their efforts to construct more imidazole moiety. From the above observation, development of more practical and versatile method from the available resources is one of the most vital features.

Thus in this study, we aim to synthesize a novel derivative of 1-(2,3-dihydrobenzo[b][1,4]dioxin-6-yl)-2-(furan-2-yl)-4,5-diphenyl-1H-imidazole (DDFDI)compound in one-pot reaction of 2,6-bis(4-chlorophenyl)-3-methylpiperidine-4-one, acetic acid and

* Corresponding author.
E-mail address: rajaraman4389@gmail.com (D. Rajaraman).

https://doi.org/10.1016/j.molstruc.2022.134314
0022-2860/

2,4,6-trichlorophenyl)hydrazine in the presence of ethanol as a catalyst. The prediction of molecular geometry parameters, HOMO-LUMO orbitals, intramolecular charge transfer, NBO activity and molecular electrostatic potential (MEP) of the target molecule were carried out in B3LYP/6-31G (d,p) level of theory to study all the reactivity and biological importance of the target compound. The DDFDI compound has been experimented in the molecular docking studies and found better binding results in the pharmaceutical arena than the target drugs.

2. Experimental

2.1. General method

All the chemicals and solvents were purchased from Sigma Aldrich and chemical suppliers, used as received without further purification. The DDFDI compound was recorded by the Fourier transform-infrared (FTIR) spectra in the range of 4000-400cm^{-1} using AVATAR 300FTIR. The ^{1}H-NMR and ^{13}C-NMR spectra of the title compound were recorded at 400MHz on Bruker AMX 400MHz spectrometer and 100MHz on BRUKER AMX400MHz spectrometer using Dimethyl sulfoxide ($DMSO_4$) as a solvent. The melting points were verified by open capillaries and uncorrected.

2.2. Computational method

In the present work, quantum mechanical calculations were performed with Gaussian-03 program. At the very first step of DDFDI calculations, the geometry occupied from the preliminary structure was fully optimized by density functional theory (DFT) using the Becke3-Lee-Yang-Parr (B3LYP) with standard 6-31 G (d, p) as the basis set [21,22].

2.3. Molecular docking studies

Molecular docking recreation was performed with the Argus Lab 4.0. The readied 3D structures of different protein was downloaded from the protein information bank (see http//www.rcsb.org/pdb) and tying webpage was made by picking "Making tying website for this protein" alternative. The ligand was then presented and docking figuring was permitted to run utilizing shape-based pursuit calculation and A Score scoring capacity. The scoring capacity is in charge of assessing the vitality between the ligand and protein target. Adaptable constructing so as to dock was permitted lattices over the coupling locales of the protein and vitality based turn is set for that ligand gathering of molecules that do not have rotatable bonds. For every pivot, torsions and made and postures (adaptation) are created amidst the docking process. For every perplexing 10 free runs were led and one posture was returned for every run. The best docking model was chosen by least tying vitality computed by Argus lab and the most suitable tying adaptation was chosen on the premise of hydrogen security connection between the ligand and protein close to the substrate tying site. The most minimal vitality postures show the most elevated tying proclivity as high vitality creates the temperamental adaptations. The subsequent receptor model was spared to Brookhaven PDB document from the record the 2D and 3D connections are seen in revelation studio 4.5 renditions [23].

2.4. Drug likeness and ADMET prediction

Drug likeness and ADMET are the current vital method to predict the potential drug candidates. At first, it emerged for the preliminary assessment of the pharmacokinetics, physicochemical and drug likeness parameters in the drug discovery process. ADMET outlooks for Absorption, Distribution, Metabolism, Excretion and toxicity. Prediction of the drug likeness of the title compound was evaluated by rule based filters from Lipinski, Ghose, veber, Egan, Muegge and synthetic accessibility difficulty level was from 1-10 [24].

2.4.1. Synthesis of the 1-(2,3-dihydrobenzo[b][1,4]dioxin-6-yl)-2-(furan-2-yl)-4,5-diphenyl-1H-imidazole (DDFDI) compound

A mixture benzil (6.0mmol), ammonium acetate (24.0mmol), 2,3-dihydrobenzo[b][1,4]dioxin-6-amine (27.0mmol) and furan-2-carbaldehyde (9.0mmol) in absolute ethanol (20ml) in the presence of $C_4H_{10}BF_3O$ (2/3drops) as a catalyst. The reaction mixture was refluxed for about 24hrs at the boiling point of ethanol (78°C) and upon completion of the reaction, the reaction mixture was cooled and Thin Layer Chromatography is a technique used to isolate non-volatile mixtures. The experiment is conducted on a glass which is coated with a thin layer of adsorbent material. The material usually used is aluminium oxide.. Thin layer chromatography (TLC) technique was monitored by using ethyl acetate: benzene (2:8) as the eluent. The reaction mixture was extracted with dichloromethane and the product was purified by column chromatography. The final product was recrystallized from ethanol by slow evaporation and harvested the pure compound of 1-(2,3-dihydrobenzo[b][1,4]dioxin-6-yl)-2-(furan-2-yl)-4,5-diphenyl-1*H*-imidazole (DDFDI).

2.4.2. Synthesis of the 1-(2,3-dihydrobenzo[b][1,4]dioxin-6-yl)-2-(furan-2-yl)-4,5-diphenyl-1H-imidazole (DDFDI)

White solid: m.p. = 178-190°C and yield 92%: IR (Neat, cm^{-1});1599 (C=N), 1245 (C-O), 1441, 1403, 1294 (C=C), 2319-3052 (C-H),^{1}H-NMR ($CDCl_3$, ppm);4.39 (m, CH_2benzodioxane), 6.34(d, H-20, furfural moiety), 6.71 (d, H-22, furfural moiety),7.14-8.53ppm (aromatic proton).^{13}C-NMR ($CDCl_3$, ppm);53.29, 64.33 ($2CH_2$, benzodioxane), 109.25, 111.33, 123.02 (carbon signal for furfural moiety), 156 (C=N), 124.04-141.31(aromatic carbon). Chemical Formula: C27H20N2O3, Exact Mass: 420.15 Molecular Weight: 420.46 m/z: 420.15 (100.0%), 421.15 (29.5%), 422.15 (5.0%) Elemental Analysis: C, 77.13; H, 4.79; N, 6.66; O, 11.42.

3. Result and discussions

3.1. Chemistry

A schematic diagram of compound DDFDI is shown in Scheme 1. The FT-IR spectral analysis of the DDFDI compound is discussed below. Generally, imines indicate a strong C=N stretching vibration in the region 1500-1600cm−1. The DDFDI compound demonstrate strong absorption band and were detected in the region 1541-1618cm−1 due to the functional group of imine. The C=N stretching band appears at 1599cm−1 in DDFDI compound showed high absorption band. The existence of C=N stretching band supports the skeleton of the imidazole ring. A concrete absorption band appeared at 1245cm−1 due to furan and dioxin C-O stretching. The aromatic C-H stretching band arises in the broad region 2319-3052cm−1. The observed imine, aliphatic and aromatic C-H stretching frequencies were confirmed the compound DDFDI.IRspectral values of compound DDFDI is displayed in Fig. 1.

1H-NMR spectra of DDFDI have been recorded in CDCl3 solvent. The signals were obtained in the 1H-NMR spectra were consigned and established accordingly to their position, multiplicities and integral values. In general, the aromatic proton signals emerged in the higher frequency region at 7.00ppm due to the magnetic anisotropic effect. In the 1H-NMR spectrum of DDFDI compound, the signals appeared in the region7.14-8.53ppm resemble to sixteen protons integral due to aromatic protons. A multiplet peak

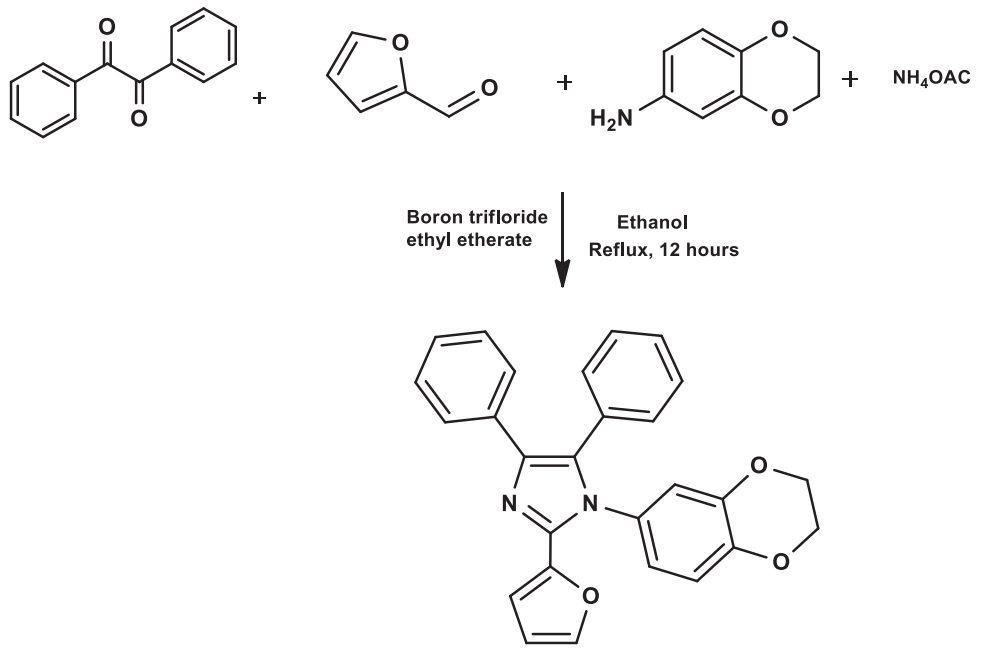

Scheme 1. Pathway for the Synthesis of 1-(2,3-dihydrobenzo[b][1,4]dioxin-6-yl)-2-(furan-2-yl)-4,5-diphenyl-1*H*-imidazole.

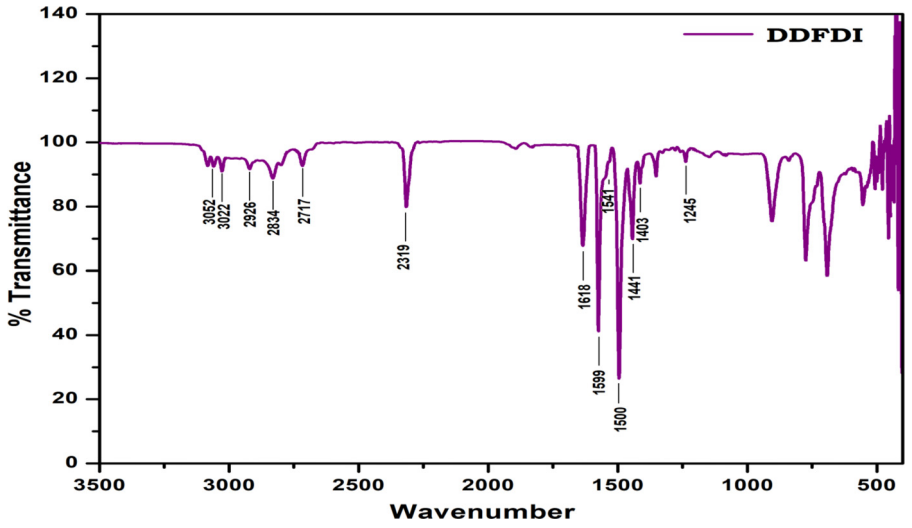

Fig. 1. FT-IR spectrum of compound DDFDI.

detected at 4.39ppm is assigned to two CH2 protons (2CH2 forbenzodioxane moiety). A douplet peak detected at 6.34ppm is assigned to H-20 proton signal of furfuryl moiety. A doublet peak was appeared at 6.71ppm was assigned to H-22 proton signal for furfural moiety.1H-NMRspectral values of compound DDFDI is displayed in Fig. 2.

The 13C-NMR spectra of 1-(furan-2-yl)methyl)-4,5-diphenyl-2-(p-tolyl)-1H-imidazole have been recorded. The 13C-NMR chemical shifts are quoted after rounding off to one decimal point. The 13C-NMR spectrum of compound DDFDIwas recorded at 400MHZ instrument.In 13C-NMR spectrum of compound DDFDI, the two CH2 carbon signals of benzodioxane moiety appeared at 53.29ppm and 64.33ppm. The C-8, C-9 and C-10 carbon signals were appeared at 109.25, 111.33 and 123.02ppm due to furfural moiety. The aromatic and ipso-carbon signals are appeared in the region of 124.04-141.31ppm. The imidazole compound containing C=N carbon signal appeared at 156.02ppm.13C-NMR spectral values of compound DDFDI is displayed in Fig. 3.

4. Geometry optimization of DDFDI compound

The DDFDI compound was computed in Gaussian 03 software package using functional B3LYP at 6-31G (d,p) as the basic level theory. The substitution of functional groups in this compound, electron donor and electron acceptor are observable in the wavelength and oscillator strengths. In DDFDI compound, the bond lengths are observed in C30-O29, C24-N27, C24-N26, C38-O50, C23-N27, C45-O49 and C25-C23 are 1.45Å, 1.33Å, 1,52Å, 1.42Å, 1.44Å, 1.43Å and 1.49Å respectively. The bond angles in C31-C30-O29, C30-O29-C28, C28-C24-N27, C24-N27-C23, C24-N26-C25, C46-O50-C38, C45-O49-C39 and C40-C39-O49 are 111.49°, 102.52°, 123.43°, 102.25°, 98.79°, 112.64°, 112.61° and 120.11° respectively.

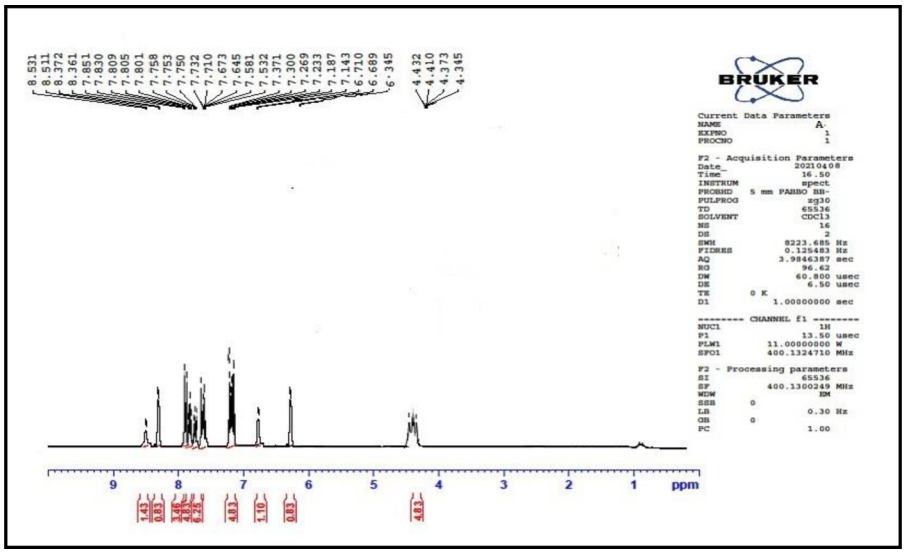

Fig. 2. ^{1}H NMR spectrum of compound DDFDI.

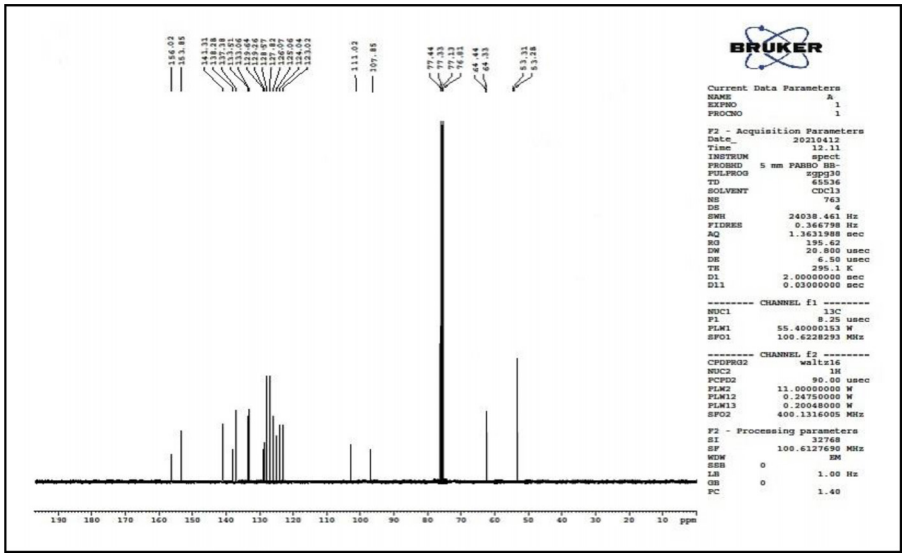

Fig. 3. ^{13}C NMR spectrum of compoundDDFDI.

While the dihedral angles at H33-C30-O29-C28, N27-C24-C25O29, C2-C25-C23-N27, N26-C24-C28-O29, C36-C37-C38-O50, H47-C45-O49-C39, C41-C40-C39-O49 and H48-C46-O50-C38 are identified at 167.79°, 0.79°, -129.85°, 178.79°, 176.15°, 170.90°, 176.21° and 170.82° respectively. When we compared our theoretical (DFT) values with experimental values of bond lengths O1-C23, N1-C7 and N2-C22 are 1.35Å, 1.32Å and 1.44Å, the bond angles are C23-O1-C26, C7-N1-C8 and C7-N2-C22 are 105.90°, 105.84° and 126.23° and the dihedral angles of N2-C15-C16C17 and O1-C23-C24-C25 are 96.00° and -2.05° respectively were found to be alike [23]. From this observed bond length, bond angle and dihedral angle, the compound (FMDI) have planar geometry. The optimized structure of DDFDI compound is shown in Fig. 4. The optimized parameters namely bond lengths, bond angles and dihedral angles are of an isolated molecule in gaseous phase (Table 1).

4.1. Natural bond orbital

Natural bond orbital (NBO) is a special technique to study intramolecular and intermolecular bonding, hybridization, interaction bonding and charge transfer in the molecular structure [23]. The NBO calculation was carried out in the Gaussian 03 package at the DFT/B3LYP level using 6-31G (d,p) as the basis set to recognize numerous second order interactions between occupied orbitals and unoccupied orbitals is shown in Table 2. The second order Fock matrix was performed to calculate the donor-acceptor interactions in the NBO analysis. For each donor (i) and acceptor (j), the stabilization energy E2 is related with the delocalization i-j is estimated as

$$E^2 = \Delta E_{ij} = qi\frac{F(i.j)^2}{\in j - \in i}$$

Where q_i = donor orbital occupancy
ε_i and ε_j = diagonal elements
F (i, j) = off diagonal NBO Fock matrix element.

The stabilization energy (E^2) values verified the hyperconjugative interaction and charge transfers by the orbital overlap were determined between πC_{28}-C_{32} to $\sigma^* C_{37}$-H_{42} for anti-bonding orbital with stabilization energy 81.59kJ/mol. The larger energy value of E^2 gives more chemical stability in the molecular interaction between electron donors and electron acceptors [25].

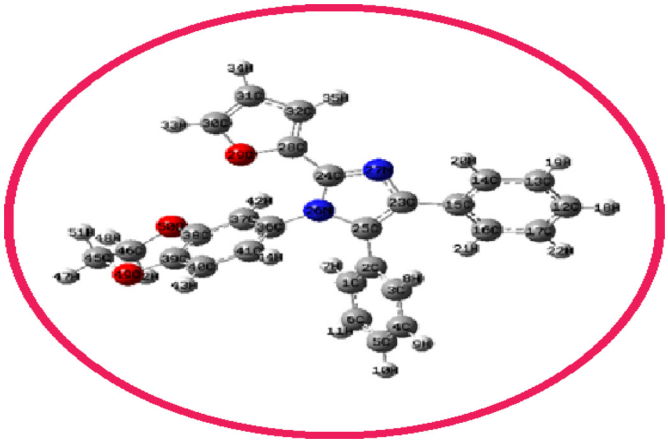

Fig. 4. Optimized structure of DDFDI compound.

Table 1
Selected bond lengths (Å), bond angles (°) and torsional angles (°) of DDFDI compound by DFT.

Bond Lengths	DFT	Dihedral angle	DFT
30C-29O	1.45	33H-30C-29O-28C	167.79
28C-29O	1.45	31C-30C-29O-28C	-12.06
24C- 27N	1.33	30C-29O-28C-32C	12.04
23C-27N	1.44	30C-29O-28C-24C	-167.83
24C-26N	1.52	27N-24C-28C-29O	0.79
36C-26N	1.46	33H-30C-29O-28C	167.79
25C-26N	1.45	1C-2C-25C-26N	91.60
38C-50O	1.42	14C-15C-23C-27N	93.50
46C-50O	1.43	36C-37C-38C-50O	176.15
45C-49O	1.43	42H-37C-38C-50O	-3.51
39C-49O	1.35	37C-38C-50O-46C	158.82
25C-23C	1.49	38C-50O-46C-45C	51.121
Bond Angles		48H-46C-50O-38C	170.82
31C-30C-29O	111.49	49O-39C-38C-50C	6.16
33C-30C-29O	124.24	47H-45C-49O-39C	170.90
30C-29O-28C	102.52	51H-45C-49O-39C	-69.17
32C-28C-29O	111.49	39C-49O-45C-46C	51.19
24C-28C-29O	124.22	40C-39C-49O-45C	158.74
28C-24C-27N	123.43	41C-40C-39C-49O	176.21
24C-27N-23C	102.25	16C-15C-23C-27N	-56.81
26C-24C-27N	113.04	41C-36C-26N-24C	-145.89
15C-23C-27N	127.93	41C-36C-26N-25C	-34.12
25C-23C-27N	103.75	1C-2C-25C-26N	91.60
24C-26N-25C	98.79	14C-15C-23C-27N	93.50
23C-25C-26N	100.62	36C-37C-38C-50O	176.15
40C-39C-49O	120.11	42H-37C-38C-50O	-3.51
51H-45C-49O	110.49	37C-38C-50O-46C	158.82
36C-26N-24C	112.60	38C-50O-46C-45C	51.121
41C-36C-26N	119.88	1C-2C-25C-26N	91.60
37C-36C-26N	120.19	14C-15C-23C-27N	93.50
46C-50O-38C	112.64	36C-37C-38C-50O	176.15
37C-38C-50O	120.16	48H-46C-50O-38C	170.82
39C-38C-50O	119.73	49O-39C-38C-50C	6.16
52H-46C-50O	110.50	47H-45C-49O-39C	170.90
Dihedral angle		51H-45C-49O-39C	-69.17
48H-46C-50O-38C	170.82	39C-49O-45C-46C	51.19
49O-39C-38C-50C	6.16	40C-39C-49O-45C	158.74
47H-45C-49O-39C	170.90	41C-40C-39C-49O	176.21
51H-45C-49O-39C	-69.17	43H-40C-39C-49O	-3.05

4.2. The frontier molecular orbitals

The highest occupied molecular orbitals (HOMO's) and lowest unoccupied molecular orbitals (LUMO's) are the types of frontier molecular orbitals. The HOMO has capacity to donate an electron whereas LUMO represents the ability to accept electron. These orbitals are important to decide the stability of the chemical compound. The HOMO and LUMO energy values was calculated through DFT method using B3LYP/6-31G (d,p) level of theory are shown below.

Table 2
Significant delocalization energies of second order perturbation theory analysis of Fock matrix in NBO for compound DDFDI.

Table	Donor (i)	Acceptor (j)	E2KJ/Mol
π-σ^*	C28-C32	C37-H42	81.59
σ-π^*	C37-H42	C28-C32	66.27
n-π^*	LP(1)-O50	C37-C38	21.25
n-π^*	LP(1)-O49	C39-C40	20.33
n-π^*	LP(1)-O29	C30-C31	19.89
π-σ^*	C13-C14	C15-C16	11.25
π-π^*	C15-C16	C12-C17	10.71
π-π^*	C1-C2	C5-C6	10.49
π-π^*	C37-C38	C39-C40	10.43
π-π^*	C39-C40	C36-C41	10.17
σ-σ^*	C40-C41	C39-O49	6.15
σ-σ^*	C41-H44	C36-C37	5.79
σ-σ^*	C23-C25	N26-C36	3.98
σ-σ^*	C4-C5	C6-H11	2.99
σ-σ^*	C12-C17	C16-C17	1.31
σ-π^*	C25-N26	C24-N27	0.51

$$HOMO = -0.222eV,\ LUMO = -0.017eV$$

$$HOMO - 1 = -0.224eV,\ LUMO - 1 = -0.026eV$$

$$HOMO - 2 = -0.226eV,\ LUMO - 2 = -0.028eV$$

Their main energy gap = 0.205eV, 0.198eV, 0.198eV.

The transfer of electron from ground state to the excited state is labelled by one electron from highest occupied molecular orbitals to the lowest unoccupied molecular orbitals. As we can see from the given figure, HOMO shows the charge density contained over the entire phenyl ring. The LUMO part is situated on imidazole, furfuraldehyde and 1,4-benzodioxan-6-amine ring.The displayed diagram of HOMO-LUMO energy value is shown in Fig. 5. The energy gap between HOMO and LUMO gives the detail interaction between the molecules and chemical stability [26].

4.3. Molecular electrostatic potential

The map of molecular electrostatic potential delivers the isosurface values with the position of positive and negative electrostatic potentials and broadly used for electrophilic reactions, nucleophilic reactions, biological process, hydrogen bonding and intermolecular interactions. MEP map of the DDFDI compound was calculated by DFT method at B3LYP/6-31G (d,p) as the level of theory. The various values of the electrostatic potential at the surface are symbolized by different colours i, e, red colour denotes negative charge, partial blue colour indicate positive charge, yellow colour shows electron rich region and white colour represents region of zero potential [27]. In the present work, molecular geometry and anharmonic vibrational spectra of o-, m-, p-iodonitrobenzene have been studied. The anharmonic frequencies were calculated using second order perturbative (PT2) approach with basis set 3-21G/ on iodine and 6-311G(d,p) on other atoms at DFT(B3LYP) level of theory and were compared to experimental values. The assignments of vibrational modes of isomeric iodonitrobenzenes were done by using potential energy distribution (PED) and vibrational assignments of benzene, nitrobenzene and iodobenzene. The combination and overtone bands are also assigned. The electronic spectra were recorded as well as simulated using polarizable continuum model (PCM) at TD-B3LYP/6-311G(d,p)/3-21G/ level of theory. The vibrational and electronic spectra are interpreted. Moreover, atomic charges, MEP mapping, HOMO–LUMO, NBO analysis and various thermodynamics and molecular properties are reported. The MEP

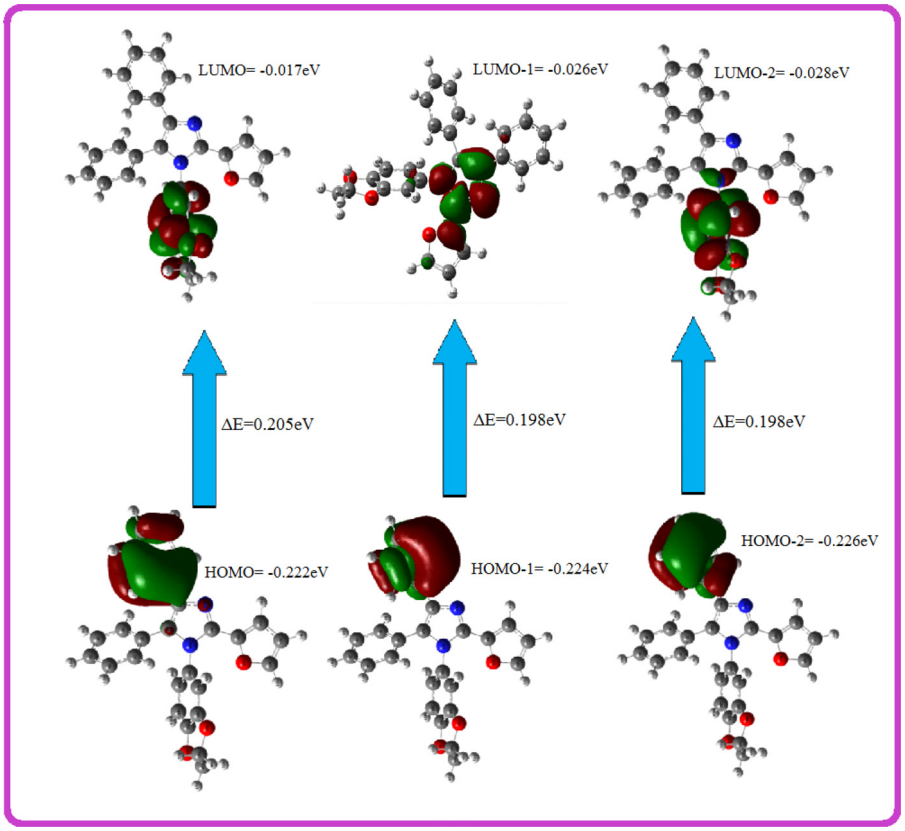

Fig. 5. Frontier Molecular orbitals HOMO-i and LUMO-i where i=1,2 with their orbital energies (eV) and orbital energy gap (eV).

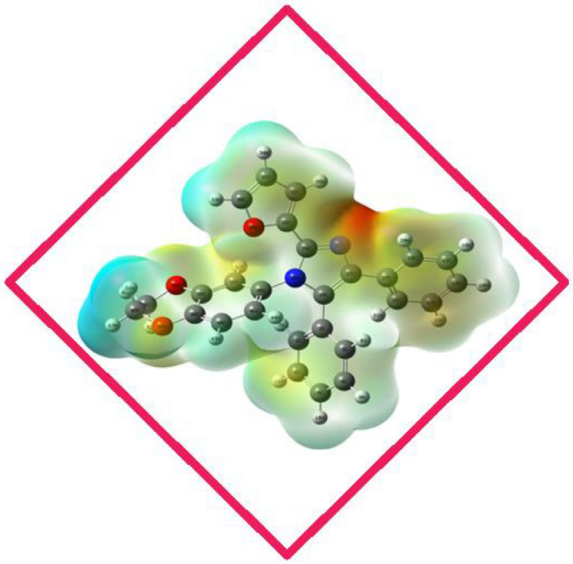

Fig. 6. Molecular electrostatic potential of DDFDI compound.

Table 3
Mulliken atomic charges of compound DDFDI.

Atom	Charge	Atom	Charge	Atom	Charge
1C	-0.10	18 H	0.09	35 H	0.19
2 C	-0.02	19 H	0.09	36 C	0.27
3 C	-0.06	20 H	0.10	37 C	-0.29
4 C	-0.10	21 H	0.10	38 C	0.29
5 C	-0.09	22 H	0.09	39 C	0.33
6 C	-0.09	23 C	0.07	40 C	-0.16
7 H	0.11	24 C	0.36	41 C	-0.12
8 H	0.11	25 C	0.14	42 H	0.22
9 H	0.10	26 N	-0.54	43 H	0.10
10 H	0.09	27 N	-0.44	44 H	0.11
11 H	0.10	28 C	0.29	45 C	0.03
12 C	-0.08	29 O	-0.50	46 C	0.03
13 C	-0.09	30 C	0.15	47 H	0.11
14 C	-0.08	31 C	-0.11	48 H	0.11
15 C	0.07	32 C	-0.19	49 O	-0.54
16 C	-0.12	33 H	0.13	50 O	-0.54
17 C	-0.09	34 H	0.11	51 H	0.12
				52 H	0.12

map shows the chemical active location and chemical reactivity of atoms as shown in Fig. 6.

4.4. Mulliken atomic charges

Mulliken atomic charge plays a significant role in the application of quantum chemical calculation to molecular system. In the mulliken atomic charge calculations, atomic charges affect the dipole moment, polarizability, electronic structure and the properties of molecular systems. The compounds DDFDI are calculated mulliken atomic charge are recorded in Table 3. Thus, from the distribution charge calculation, we can see all the heteroatoms displayed major electron density. Therefore, from the given table …the carbon atoms C1, C2, C3, C4, C5, C6, C12, C13, C14, C16, C17, C31, C32, C37, C40 and C41 possess small negative charges whereas carbon atoms C15, C23, C24, C25, C28, C36, C38, C39, C45 and C46 possess positive charges. The DDFDI compound illustrated that the high positive charges in a molecule are C24=0.36 and C39=0.33. The positive regions are associated to nucleophilic reactivity. These data clearly demonstrate that compound DDFDI are the most reactive parts taking place towards substitution reactions [28].

Table 4
The molecular electric dipole moment μ (Debye), polarizability ($\alpha 0$) and hyperpolarizability ($\beta 0$) values of compound DDFDI.

Parameters	B3LYP/6-31G (d,p)
Dipole moment (μ) Debye	
μ_x	-5.1259
μ_y	-1.8690
μ_z	-0.1353
μ	5.4577
Polarizability (α_0) x10^{-30}*esu*	
α_{xx}	418.346
α_{xy}	-6.160
α_{yy}	357.150
α_{xz}	11.928
α_{yz}	3.255
α_{zz}	183.427
α_0	0.8366 × 10^{-30}esu
Hyperpolarizability (β_0) x10^{-30}*esu*	
β_{xxx}	-217.6981
β_{xxy}	-17.9365
β_{xyy}	-30.3561
β_{yyy}	25.8286
β_{xxz}	-37.5228
β_{xyz}	-16.7069
β_{yyz}	-2.0225
β_{xzz}	-28.7195
β_{yzz}	-17.2204
β_{zzz}	7.9625
β_0	2.407 × 10^{-30}esu

4.5. Nonlinear optics

The hyperpolarizability (β_0), dipole moment (μ) and polarizability (α) of the title compound were calculated using DFT method with 6-31G (d,p) as the level of theory. The entire equations for calculating the total dipole moment (μ), polarizability (α) and first hyperpolarizability(β_0) using x, y, z components from Gaussian 03W output is shown below:

$$\mu = (\mu_x^2 + \mu_y^2 + \mu_z^2)^{1/2}$$

$$\alpha_0 = (\alpha_{xx} + \alpha_{yy} + \alpha_{zz})^{1/3}$$

$$\beta_0 = (\beta_x^2 + \beta_y^2 + \beta_z^2)^{1/2}$$

herefore, the higher values of dipole moment, polarizability and hyperpolarizability ($\beta 0$) are the efficient potential in NLO materials are shown in Table 4. Our current work reveals that the π-π interactions give more intra-molecular interaction and hence the polarizability of the molecule increases. The $\beta 0$ value of the DDFDI (2.40 × 10−30esu) compound is ∼7 times greater than that of urea (0.3728 × 10−30esu) [28]. Thus, we can say that the DDFDI compound has more potential in nonlinear optical properties.

5. Molecular docking studies

The molecular docking analysis of DDFDI ligand with COVID-19/6W41, COVID-19/6WCF, COVID-19/6Y84 and COVID-19/6W4B receptors was performed. For structure-based drug design, the molecular docking plays an important role in the biological studies and to understand the ligand receptor interactions. The particular treatment for COVID-19 is vacant till date, so from researchers many antiretroviral drugs against COVID-19 were reported and existing such as Atazanavir, Darunavir ritonavir, lopinavir, oseltamivir, remdesivir, chloroquine and hydroxyl chloroquine. Some of the imidazole drugs also reported against COVID-19 [29]. We decided to do molecular docking analysis of DDFDI compound that we can recommend against COVID-19. The molecular docking mechanism between DDFDIligand and the COVID-19/6W41, COVID-19/6WCF, COVID-19/6Y84 and COVID-19/6W4B receptor was examined and evaluated. Firstly, 6W41 is Crystal structure of SARS-CoV-2 receptor binding domain in complex with human antibody CR3022. In the binding mode, the DDFDI compound was attractively bound to 6W41 via Vander Waals, carbon hydrogen bond, π-sigma, π-lone pair, π-π T-shaped, π-alkyl bond interactions. The residue ALA621, CYS490 is binding with phenyl group in the imidazole ring with distance 6.33Å, 4.13Å by π-alkyl bond. The residue LYS246 attached in phenyl ring, imidazole and furan ring having a bond distance 4.65Å, 4.66Å, 4.33Å by Vander Waals bond. The residues LEU489, ILE244, LEU616 is binding with phenyl, imidazole and furan moiety with various bond distance 5.01Å, 5.09Å, 5.12Å,4.77Å, 4.17Å, 5.65Å by π-sigma bond. The residue HIS618 is binding with dioxane moiety having a bond distance of 4.84Å, 3.13Å, 6.55Å by π-lone pair bond. But, the standard drug hydroxylchloroquine is enclosed with carbon-hydrogen bond, mixed alkyl and Pi-alkyl bond interactions of the amino acids GLU438 (3.45, 3.08), PHE441, VAL466, LEU467, PHE473, TRP535 residues having a bond distance 4.07Å, 5.09Å, 4.38Å, 4.89Å, 3.39Å and 6.12Å via π-alkyl and alkyl bond. The binding energy of DDFDI compound is -11.08kcal/mol while the standard drug (hydroxyl chloroquine) is - 9.21kcal/mol. The Docking of 2D and 3D images of compound DDFDI and standard drug (hydroxylchloroquine) with 6W41 receptor were shown in Fig. 7.

Secondly, the interactions between DDFDI ligand and 6WCF receptor. 6WCF is a Crystal Structure of ADP ribose phosphatase of NSP3 from SARS-CoV-2 in complex with MES. SARS-CoV-2 main protease has a vital role in the processing of polyprotein that is translated from viral RNA, and the protease is considered as the main role for viral survival and growth. The compound was well bound to 6WCF via π-π stacked, amide-π stacked, π-sigma and Vander Waals. The π-π stacked, amide-π stacked interactions of the amino acids GLY47, PHE132, ALA38 have bond distance 3.96Å, 3.18Å and 4.67Å is binding with phenyl moiety. The amino acids ILL131 have bond distance 5.19Å, 4.01Å, 3.05Å, 5.40Å, 2.50Å is binding with furan, imidazole, phenyl and dioxane moiety via π-sigma. The Vander Waals has bond distance 2.08Å of GLY130 residue is attached to dioxane moiety. But the standard hydroxylchloroquine is enclosed with mixed alkyl and π-alkyl interactions, conventional hydrogen bond and π-lone pair between ligand and receptor. The residues ALA129, LEU126, VAL49, ILE131 are attached to methyl ring and chorophenyl moiety have bond distance 3.03Å, 4.53Å, 4.93Å, 4.68Å via alky and π-alkyl interactions. The amino acids of ASP157, PHE156 with a bond distance 2.98Å, 2.67Å is attached with oxane moieties. The residue of PHE132 have bond distance 3.62Å, 2.84Å is attached to pyridine and chlorophenyl moiety via π-lone pair bond. The binding energy of compound DDFDI is -9.75kcal/mol while the standard drug (hydroxyl chloroquine) is - 8.31kcal/mol. The docked 2D and 3D images of compound DDFDI and standard drug (hydroxyl chloroquine) with 6WCF receptor were shown in Fig. 8.

Thirdly, the interactions between DDFDI ligand and 6Y84 receptor. 6Y84 is the COVID-19 main protease with un-liganded active site. SARS-CoV-2 main protease has a vital role in the processing of polyprotein that is translated from viral RNA, and the protease is considered as the main role for viral survival and growth. The compound was well bound to 6Y84 via π-donor hydrogen bond and π-π T-shaped. The pi-donor hydrogen bond and π-π T-shaped interactions of the amino acids TYR101 (2.81Å) and PHE103 (3.61Å) is binding with phenyl moiety. But the standard hydroxylchloroquine is enclosed with Vander Waals, carbon hydrogen bond, mixed alkyl and π-alkyl interactions between ligand and receptor. The residues PHE294 is attached to pyridine and chlorophenyl moiety have bond distance 4.16Å, 3.18Å and 3.27Å via carbon hydrogen bond. The amino acids of PRO293, ILE249, CYS300, LEU253, VAL297, PRO252 with a bond distance 4.64Å, 3.55Å, 4.01Å, 5.12Å, 4.73Å, 3.50Å,

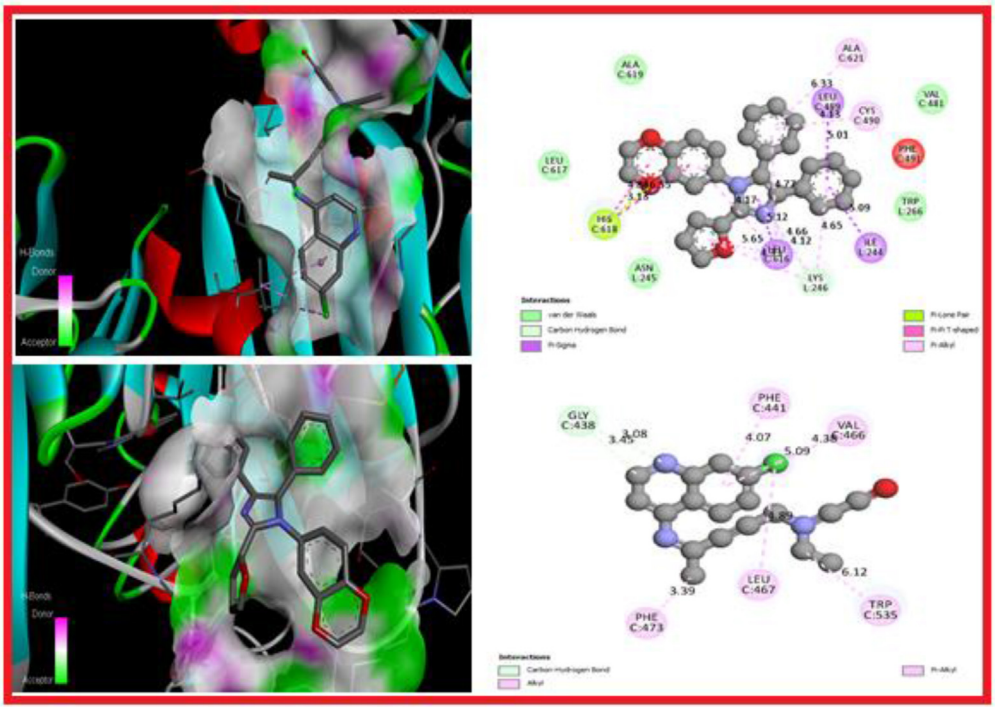

Fig. 7. The 2D and 3D images of compound DDFDI and standard drug (hydroxyl chloroquine) with 6W41 receptor.

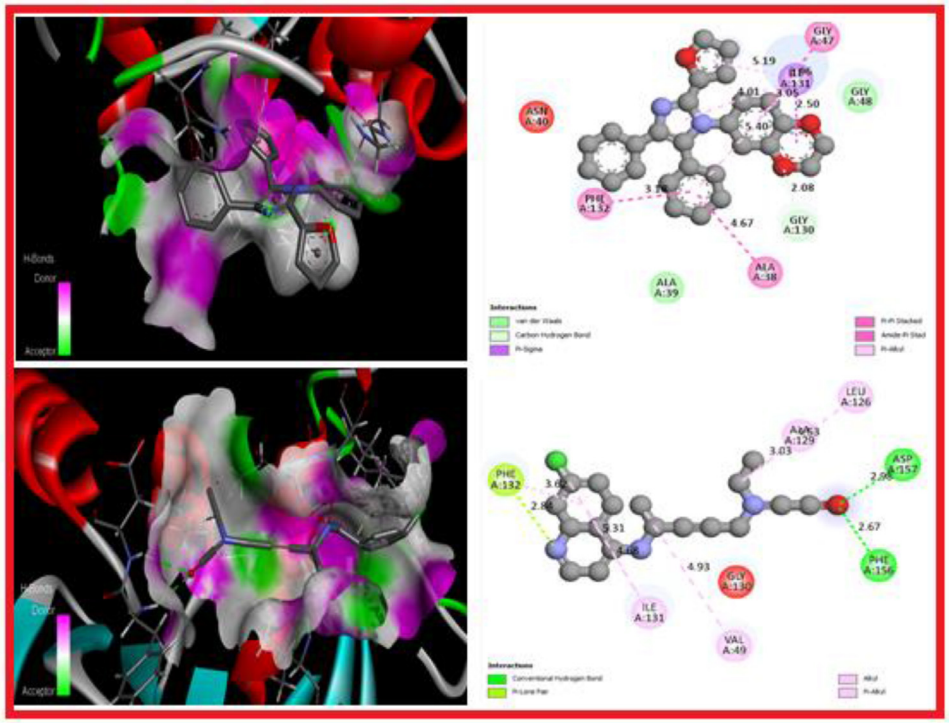

Fig. 8. The 2D and 3D images of compound DDFDI and standard drug (hydroxyl chloroquine) with 6WCF receptor.

6.38Å, 5.06Å, 5.28Å is attached with methyl, chlorophenyl and phenyl moieties. The binding energy of compound DDFDI is -10.62kcal/mol while the standard drug (hydroxyl chloroquine) is -8.68kcal/mol. The docked 2D and 3D images of compound DDFDI and standard drug (hydroxyl chloroquine) with 6Y84 receptor were shown in Fig. 9.

Lastly, the interactions between DDFDI ligand and the 6W4B receptor. 6W4b is the crystal structure of Nsp9 RNA binding protein of SARS CoV-2. SARS-CoV-2 main protease has a vital role in the processing of polyprotein that is translated from viral RNA, and the protease is considered as the main role for viral survival and growth. The compound was well bound to 6W4b via π-sigma, π-sulfur, π-π T-shaped and π-alkyl. The π-π T-shaped interaction of the amino acids was attached by the residue PHE91 (4.3Å) while the residue LEU89, VAL0 is attached to the phenyl group has bond distance 4.42Å, 4.20Å via π-alkyl bond. The residue CYS74,

Table 5
Binding energy values for synthesized compound DDFDI and standard drug for different proteins.

S.No	Protein (pdb Id)	Synthesized compound (DDFDI) Binding energy (kcal/mol)	Standard drug (Hydroxyl chloroquine) Binding energy (kcal/mol)
1	6W41	-11.08	-9.21
2	6WCF	-9.75	-8.31
3	6Y84	-10.62	-8.68
4	6W4B	-12.25	-10.18

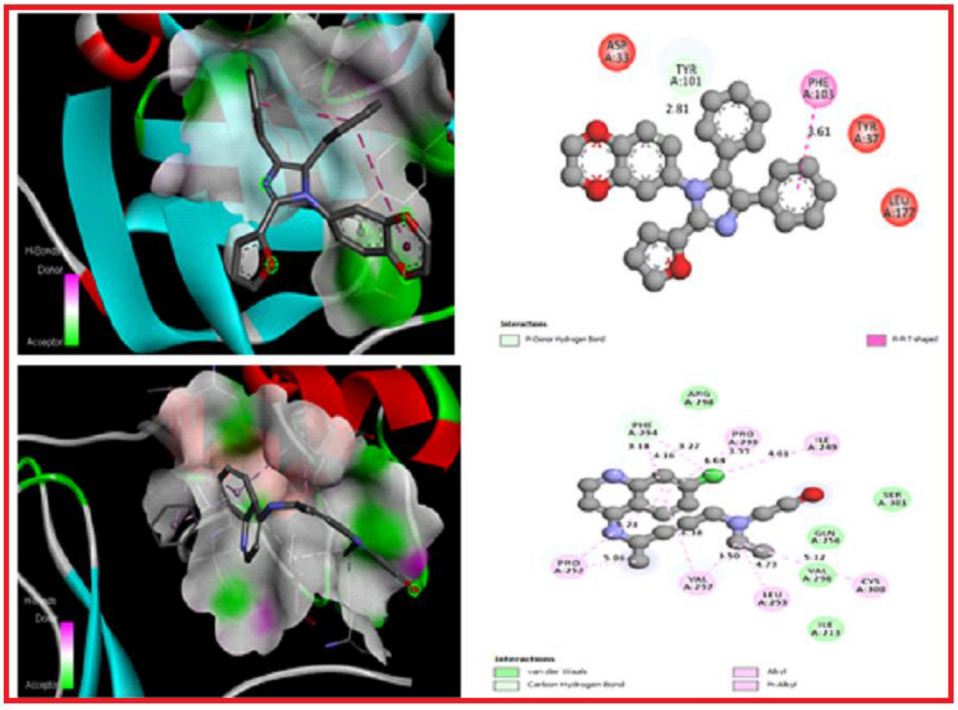

Fig. 9. The docked 2D and 3D images of compound DDFDI and standard drug (hydroxyl chloroquine) with 6WCF receptor.

MET0 is attached to phenyl ring, imidazole and furan moiety have bond distance 3.01Å, 5.10Å, 4.83Å via π-sulfur bond whereas the amino acids LEU107, LEU104, LEW5 are attached to phenyl, furan and imidazole moiety with bond distance 3.09Å, 3.76Å, 3.41Å, 4.58Å, 4.82Å, 5.09Å, 5.30Å via π-sigma bond. But the standard hydroxylchloroquine is enclosed with alkyl and π-alkyl interactions between ligand and receptor. The residues PHE76, LEU46, ALA79, LEU5, LEU113, LEU104, VAL111, LEU107 with bond distance 4.13Å, 3.68Å, 4.64Å, 4.26Å, 4.64Å, 4.54Å, 3.13Å, 3.68Å, 5.15Å, 3.77Å, 5.01Å, 4.58Å were attached to phenyl, chlorophenyl and methyl moiety. The binding energy of compound DDFDI is -12.25kcal/mol while the standard drug (hydroxyl chloroquine) is -10.18kcal/mol. The docked 2D and 3D images of compound DDFDI and standard drug (hydroxyl chloroquine) with 6Y84 receptor were shown in Fig. 10. The binding energy values for synthesized compound DDFDI and standard drug for different proteins are shown in Table 5. From the above molecular docking results, we concluded that DDFDI compound can be considered as potential agent against COVID-19/6W41/6WCF/6Y84/6W4b receptors (Table 4).

6. ADMET prediction and drug likeness

Computational techniques and prediction of the various physicochemical and pharmacokinetics of novel drug candidate is one of the angle for the drug development process to save time, effort and cost. The word drug-likeness indicated the stability between the structure characteristic and various molecular properties which determine the drug discovery and production. The five rules of Lipinski plays the main role in the discovery of drugs and in this designed compound the five rules were employed to determine the bioavailability of bulk materials to examine the drug-likeness properties and the results shows no violation of the rule. The physicochemical properties with their ranges as described by the Lipinski's rule of five which includes; Molecular weight is found to be 420.45g/mol (<500g/mol), hydrogen bond donor is 0 (<5), hydrogen bond acceptor is 4 (<5), High lipophilicity LogP is 4.93 (<5), Van der Walls topological polar surface area (TPSA) value is 49.42Å^2(120Å^2). Hence, the compound DDFDI obeys the five rules of Lipinski's. The ADMET of the designed compound were used admet SAR database (http://lmmd.ecust.edu.cn/admetsar1/predict). The features of ADMET properties of the title compound to act as drug leads such as blood-brain barrier (BBB) penetration and gastrointestinal absorption (GI), water soluble capability, lipophilicity and CYP1A2 inhibitor. The ADMET result shows that the studied compound has well absorbed by the gastrointestinal tract and easily flow into the brain to reach the target enzyme. Similarly, the effect of cytochrome P450 enzymes (CYP1A2, CYP2C19 and CYP3A4) for drug metabolism in humans and the toxicity properties were non-inhibitors of CYP2C9 and CYP2D6 cytochrome P450 enzymes. Skin permeability is considered in transdermal drug delivery and evaluates product efficacy, the studied compound show low skin permeability at -4.98cm/s. Here, skin permeability shows that the compound has the ability to reduce skin allergy when directed and the results proved that

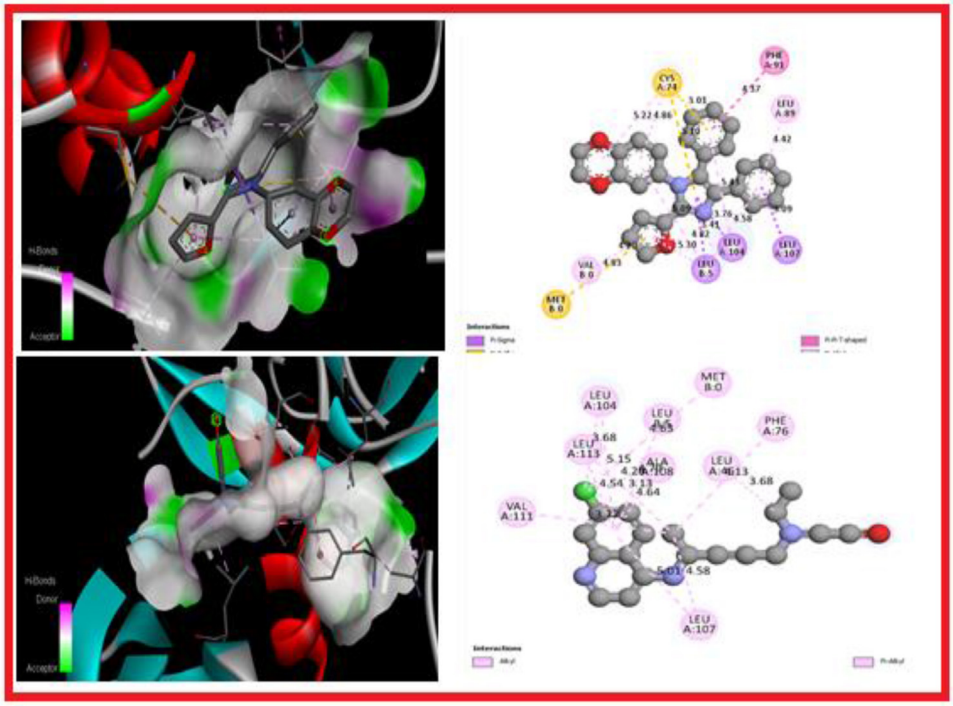

Fig. 10. The docked 2D and 3D images of compound DDFDI and standard drug (hydroxyl chloroquine) with 6W4b receptor.

the compound is harmless and cure for skin allergies [30–32]. The ADMET prediction results of compound are given in Table 6.

7. Conclusion

1-(2,3-dihydrobenzo[b][1,4]dioxin-6-yl)-2-(furan-2-yl)-4,5-diphenyl-1H-imidazole derivatives (DDFDI) have been synthesized in the presence of C4H10BF3O. The compound DDFDI have been characterized by IR, 1H-NMR and 13C-NMR spectral techniques. Theoretical calculation was carried out for compound DDFDI using DFT/B3LYP/6-31G (d,p) basis set and their optimized bond parameters were calculated.The stabilization energy (E2) values verified the hyperconjugative interaction and charge transfer by the orbital overlap were determined between π(C28-C32) to σ^*(C37-H42) for anti-bonding orbital with stabilization energy 81.59kJ/mol. The larger energy value of E2 gives more chemical stability in the molecular interaction between electron donors and electron acceptors.HOMO shows the charge density contained over the entire phenyl ring. The LUMO part is situated on imidazole, furfuraldehyde and 1,4-benzodioxan-6-amine ring. The molecular energies of HOMO, HOMO-1, HOMO-2 levels are -0.222, -0.224 and -0.226eV respectively while LUMO, LUMO+1, LUMO+2 levels are 0.017, 0.026, 0.028eV, respectively. The band gap energy between HOMO and LUMO is 0.205eV.Nonlinear optical studies revealed that the π-σ^* interactions tend more intra-molecular interaction and hence the polarizability of the molecule increases. The β0 value of the DDFDI compound is ~7 times greater than that of urea. Drug likeness predicts the oral activity and ADMET property analysis gives an idea about the pharmacokinetic properties of the title molecule. Molecular docking studies reveals that the compound DDFDI exhibit more binding energy are -11.08, -9.75, -10.62 and -12.25kcal/mol while the standard drug (hydroxyl chloroquine) is -9.21, -8.31, -8.68 and -10.18kcal/mol with different Covid-19/ 6W41/ 6WCF/ 6Y84/ 6W4B receptors. Finally, molecular docking results have shows that the compound DDFDI can be considered as a potential antiviral agent.

Declaration of Competing Interest

I declare no conflict of interest.

CRediT authorship contribution statement

D. Rajaraman: Conceptualization, Supervision, Investigation, Methodology, Resources, Formal analysis, Data curation, Writing – original draft. **L. Athishu Anthony:** Conceptualization, Investigation, Methodology, Resources, Formal analysis, Data curation, Writing – original draft. **P. Nethaji:** Software, Resources. **Ravali Vallangi:** Software, Resources.

Data availability

Data will be made available on request.

References

[1] J.J. Gabla, S.R. Mistry, K.C. Maheria, An efficient green protocol for the synthesis of tetra-substituted imidazoles catalyzed by zeolite BEA: effect of surface acidity and polarity of zeolite, Catal. Sci. Technol. 7 (21) (2017) 5154–5167, doi:10.1039/C7CY01398A.
[2] N. Jagadishbabu, K. Shivashankar, One-pot synthesis of 2,4,5-triphenyl imidazoles from 1,2-diols as key reagents: one-pot synthesis of imidazoles, J. Chin. Chem. Soc. 64 (5) (2017) 474–480, doi:10.1002/jccs.201600746.
[3] M.S. Ahmad, Synthesis and XRD, FT-IR vibrational, UV–vis, and nonlinear optical exploration of novel tetra substituted imidazole derivatives: a synergistic experimental-computational analysis, J. Phys. Chem. Solids 115 (2018) 265–276, doi:10.1016/j.jpcs.2017.12.054.
[4] M. Ghandi, P. Moshtaghi, A. Abbasi, Catalyst-free synthesis of 3-hydroxyimidazo[1,2- a]pyridine zwitterion derivatives via the three-component reaction of ethyl glyoxalate, 2–aminopyridines and cyclic 1,3-dicarbonyls, Tetrahedron Lett. 58 (19) (2017) 1887–1890, doi:10.1016/j.tetlet.2017.04.009.
[5] B. Karami, K. Eskandari, M. Farahi, A. Barmas, An effective and new method for the synthesis of polysubstituted imidazoles by the use of $CrCl_3.6H_2O$ as a green and reusable catalyst: synthasis of some novel imidazole derivatives, J. Chin. Chem. Soc. 59 (4) (2012) 473–479, doi:10.1002/jccs.201100555.
[6] G. Kumar, N.K. Mogha, M. Kumar, S. Dhanraj, T. Masram, NiO nanocomposites/rGO as heterogeneous catalysis for imidazole scaffolds with their applications in inhibiting DNA binding activity, Dalton Trans. 49 (2020) 1963–1974, doi:10.1039/C9DT04416G.

[7] A. Jayashree, B. Narayana, S. Madan Kumar, K.R. Raghi, B.K.S d, T.K. Manoj Kumar, Synthesis, X-ray crystal structure, Hirshfeld surface analysis, DFT, MESP and molecular docking studies of 2-(4-bromophenyl)-1-(3-fluoro-4-methylphenyl)-4,5-diphenyl- 1 H -imidazole, Chem. Data Collect. 21 (2019) 100237, doi:10.1039/org/10.1016/j.cdc.2019.100237.
[8] H. Alinezhad, V. Alinezhad, S. Mohseni Tavakkoli, Simple, efficient, and convenient one-pot synthesis of imidazole derivatives in the presence of nanosilica-supported imidazolium ionic liquid as a catalyst: synthesis of imidazole derivatives, J. Chin. Chem. Soc. 64 (4) (Apr. 2017) 385–389, doi:10.1002/jccs.201600764.
[9] C. Bathula, R. MK, A.K. Kc, H. Yadav, S. Ramesh, S. Shinde, N.K. Shrestha, K.M. Mahadevan, V. Reddyg, Microwave assisted synthesis of imidazolyl fluorescent dyes as antimicrobial agents, J. Mater. Sci. Technol. 9 (3) (2020) 6900–6908, doi:10.1039/org/10.1016/j.jmrt.2020.01.011.
[10] R. Babar, M.A. Munawar, M.N. Tahir, M. Arif, Synthesis and optical studies of Y-shaped imidazole derivatives, Spectrochim. Acta Part A 217 (2019) 223–236, doi:10.1039/org/10.1016/j.saa.2019.03.043.
[11] D. Rajaraman, G. Sundararajan, N.K. Loganath, K. Krishnasamy, Synthesis, molecular structure, DFT studies and antimicrobial activities of some novel 3-(1-(3,4-dimethoxyphenethyl)-4,5-diphenyl-1H-imidazol-2-yl)-1H-indole derivatives and its molecular docking studies, J. Mol. Struct. 1127 (2017) 597–610, doi:10.1016/j.molstruc.2016.08.021.
[12] R.T. Ulahannan, V. Kannan, V. Vidya, K. Sreekumar, Synthesis and DFT studies of the structure - NLO activity evaluation of 2-(4-methoxyphenyl)-1,4,5-triphenyl-2,5-dihydro-1H-imidazole, J. Mol. Struct. 1199 (2020) 127004, doi:10.1016/j.molstruc.2019.127004.
[13] N.J.P. Subhashini, E. Praveen Kumar, N. Gurrapu, V. Yerragunta, Design and synthesis of imidazolo-1, 2,3-triazoles hybrid compounds by microwave-assisted method: Evaluation as an antioxidant and antimicrobial agents and molecular docking studies, J. Mol. Struct. 1180 (2019) 618–628, doi:10.1016/j.molstruc.2018.11.029.
[14] D. Rajaraman, G. Sundararajan, R. Rajkumar, S. Bharanidharan, K. Krishnasamy, Synthesis, crystal structure investigation, DFT studies and DPPH radical scavenging activity of 1-(furan-2-ylmethyl)-2,4,5-triphenyl- 1H -imidazole derivatives, J. Mol. Struct. 1108 (2016) 698–707, doi:10.1016/j.molstruc.2015.11.084.
[15] M. Muthukkumar, et al., Redetermination of the crystal structure of 2-oxo-1,3-thiazolidin-4-iminium chloride, Acta Crystallogr. 75 (4) (2019) 443–446, doi:10.1107/S2056989019003189.
[16] S. Çağlar Yavuz, S. Akkoç, E. Sarıpınar, The cytotoxic activities of imidazole derivatives prepared from various guanylhydrazone and phenylglyoxal monohydrate, Synth. Commun. (2019) 3198–3209, doi:10.1039/org/10.1080/00397911.2019.1661481.
[17] G. Meier, M. Krause, A. Hüls, X. Ligneau, H.H. Pertz, J.-.M. Arrang, C. Robin Ganellin, J.-.C. Schwartz, W. Schunack, Holger Stark, 4-(omega-(alkyloxy)alkyl)-1H-imidazole derivatives as histamine H(3) receptor antagonists/agonists, J. Med. Chem. 47 (10) (2004) 2678–2687, doi:10.1021/jm031065q.
[18] Y. Tian, Acid-catalyzed synthesis of imidazole derivatives via N-phenylbenzimidamides and sulfoxonium ylides cyclization, Tetrahedron 75 (19) (2019) 2817–2823, doi:10.1016/j.tet.2019.04.004.
[19] H.J. Zhang, X. Qin, K. Liu, D.D. Zhu, X.M. Wang, H.L. Zhu, Synthesis, antibacterial activities and molecular docking studies of Schiff bases derived from N-(2/4-benzaldehyde-amino) phenyl-N′-phenyl-thiourea, Bioorg. Med. Chem. 19 (18) (2011) 5708–5715, doi:10.1016/j.bmc.2011.06.077.
[20] P. Wu, X. Zhang, B. Chen, Direct synthesis of 2,4,5-trisubstituted imidazoles and di/tri-substituted pyrimidines via cycloadditions of α,β-unsaturated ketones/aldehydes and N′-hydroxyl imidamides, Tetrahedron Lett. 60 (16) (2019) 1103–1107, doi:10.1016/j.tetlet.2019.03.025.
[21] K. Sarojini, H. Krishnan, C.C. Kanakam, S. Muthu, Synthesis, X-ray structural, characterization, NBO and HOMO–LUMO analysis using DFT study of 4-methyl-N-(naphthalene-1-yl)benzene sulfonamide, Spectrochim. Acta A Mol. Biomol. Spectrosc. 96 (2012) 657–667, doi:10.1016/j.saa.2012.07.037.
[22] A.W. Salman, et al., Sterically modulated palladium (II)−N-heterocyclic carbene complexes for the catalytic oxidation of olefins: Synthesis, crystal structure, characterization and DFT studies, Polyhedron 81 (2014) 499–510, doi:10.1016/j.poly.2014.06.054.
[23] L.A. Anthony, D. Rajaraman, M. Shanmugam, K. Krishnasamy, Synthesis, spectral techniques, X-ray Crystal structure, DFT method, Hirshfeld surface analysis and Molecular docking studies of 1-(furan-2-yl)methyl)-4,5-diphenyl-2-(p-tolyl)-1H-imidazole, Chem. Data Collect. 28 (2020) 100421, doi:10.1016/j.cdc.2020.100421.
[24] S.B. Olasupo, A. Uzairu, G.A. Shallangwa, S. Uba, Profiling the antidepressant properties of phenyl piperidine derivatives as inhibitors of serotonin transporter (SERT) via cheminformatics modeling, molecular docking and ADMET predictions, Sci. Afr. 9 (2020) e00517, doi:10.1016/j.sciaf.2020.e00517.
[25] C. Sridevi, G. Velraj, Investigation of molecular structure, vibrational, electronic, NMR and NBO analysis of 5-chloro-1-methyl-4-nitro-1H-imidazole (CMNI) using ab initio HF and DFT calculations, J. Mol. Struct. 1019 (2012) 50–60, doi:10.1016/j.molstruc.2012.03.040.
[26] M.J. Alam, S. Ahmad, Molecular structure, anharmonic vibrational analysis and electronic spectra of o-, m-, p-iodonitrobenzene using DFT calculations, J. Mol. Struct. 1059 (2014) 239–254, doi:10.1016/j.molstruc.2013.12.002.
[27] V. Balachandran, G. Santhi, V. Karpagam, A. Lakshmi, DFT computation and spectroscopic analysis of N-(p-methoxybenzylidene)aniline, a potentially useful NLO material, J. Mol. Struct. 1047 (2013) 249–261, doi:10.1016/j.molstruc.2013.05.021.
[28] P. Shafieyoon, E. Mehdipour, Y.S. Mary, Synthesis, characterization and biological investigation of glycine-based sulfonamide derivative and its complex: vibration assignment, HOMO – LUMO analysis, MEP and molecular docking, J. Mol. Struct. 1181 (2019) 244–252, doi:10.1016/j.molstruc.2018.12.067.
[29] V.A. Verma, A.R. Saundane, R.S. Meti, D.R. Vennapu, Synthesis of novel indolo[3,2-c]isoquinoline derivatives bearing pyrimidine, piperazine rings and their biological evaluation and docking studies against COVID-19 virus main protease, J. Mol. Struct. 1229 (2021) 129829, doi:10.1016/j.molstruc.2020.129829.
[30] Q.S. Obu, Synthesis, spectra (FT-IR, NMR) investigations, DFT study, in silico ADMET and Molecular docking analysis of 2-amino-4-(4-aminophenyl)thiophene-3-carbonitrile as a potential anti-tubercular agent, J. Mol. Struct. 1244 (2021) 130880, doi:10.1016/j.molstruc.2021.130880.
[31] N. Kavitha, M. Alivelu, Investigation of structures, QTAIM, RDG, ADMET, and docking properties of SASC compound using experimental and theoretical approach, Comput. Theor. Chem. 1201 (2021) 113287, doi:10.1016/j.comptc.2021.113287.
[32] D.A. Abdelrheem, A.A. Rahman, K.N.M. Elsayed, H.R. Abd El-Mageed, H.S. Mohamed, S.A. Ahmed, Isolation, characterization, *in vitro* anticancer activity, dft calculations, molecular docking, bioactivity score, drug-likeness and admet studies of eight phytoconstituents from brown alga sargassum platycarpum, J. Mol. Struct. 1225 (2021) 129245, doi:10.1016/j.molstruc.2020.129245.